Proceedings of the 13th International Forum of Automotive Traffic Safety, 2016,pp392-403
No.ATS.2016.421

Fracture Behavior of Aluminum Alloy 6082-T6 at Different Stress Triaxialities

Xuanzhen CHEN[1], Yong PENG[1,2], Shan PENG[1], Ping XU[1]

[1] Key Laboratory of Traffic Safety on Track of Ministry of Education, School of Traffic & Transportation Engineering, Central South University, Changsha, 410075, China
[2] State Key Laboratory of High Performance Complex Manufacturing, Central South University, Changsha, 410006, China
Email: yong_peng@csu.edu.cn

Abstract: This study aims to investigate the fracture behavior of aluminum alloy 6082-T6 (AA6082-T6) at different triaxialities. A series of tensile tests and numerical simulations based on finite element analysis (FEA) were performed. In this study, the average stress triaxiality and equivalent plastic facture strain obtained from numerical simulations were used in the calibration of J-C fracture model. To validate the calibration method,both of the J-C constitutive model and fracture model wereemployed in numerical simulations and the results was compared with experimental result. The calibrated J-C fracture model exhibits higher accuracy in predicting the fracture strain in AA6082-T6 tensile tests. Finally, the Scanning Electron Microscope (SEM) fractographs of specimens with different initial stress triaxialities were analyzed. It is shown thatthe size of dimples over the fracture surfaces likely relate to the initial stress triaxiality positively.

Keywords: Aluminum alloy 6082-T6, Johnson-Cook model, Strain rate, Stress triaxiality, Numerical simulation

1 Introduction

Aluminum alloys, with low density, high strength to weight ratio, good ductility and excellent corrosion resistance, are widely used in aviation, aerospace, automotive, machinery manufacturing etc. 6082-T6 aluminum alloy, as an Al-Mg-Si alloy, is increasingly applied to manufacture high-speed trains due to its sufficient plasticity for extrusion, relatively high strength, excellent weldability, formability and machinability. Previous studies have been carried out to investigate 6082 aluminum alloy. It is well known that aluminum alloys feature some mechanical properties, such as anisotropy and the dependence of mechanical properties on the strain rate, stress state and temperature.Spigarelli et al. [1] analyzed the peak stress dependence on strain rate and temperature based on a series of torsion tests in a wide range of temperatures and strain rates. With regard to the 6082 aluminum mechanical properties, several fruitful studies were conducted, such as Tranəet al.[2], who have evaluated the drawing efficiency of 6082 0 temper aluminum alloy for cartridge tubes. They applied the Piecewise-Linear-Plasticity constitutive model and the Cockcroft-Latham fracture criterion to the simulations. Two important conclusions were drawn in their work that the stress triaxiality ratio dominate the material failure and the constitutive model for 6082 0 temper aluminum alloy is an exponential law. For 6082 aluminum alloy in T6 temper (solution heat treatment and artificial aging), little rate sensitivity and moderated anisotropy was found by Chen et al.[3].

Fracture ductility, as the ability of a materialto bear plastic deformation without failure, is of great significance for the application of a material. Studies of effect of stress state on fracture ductility may be dated back to the research of Ludwik and Scheu[4]. They hold the view that the strength-strain curve could be given by testing tensile specimens with circumferential notches of different depths. The stress triaxiality is defined as the ratio of the hydrostatic stress and the equivalent stress to depict the stress state of materials. Tests carried out by Bridgman[5] showed that a reduced stress triaxiality could increase the fracture strain greatly. Similar conclusion was drawn by Hancock and Mackenzie[6] through a series of tensile tests on pre-notched round steel specimens.

Several failure criterions have been used in commercial FEA code by now such as LS-Dyna, Abaqus, and Ansys. The Johnson-Cook failure criterion [7] has been widely used to study the dependence of fracture strain onthe strain rate, stress triaxiality, and temperature through both experiments and numerical simulations. Considering the anisotropy of the material, Johnson-Cook failure criterions of AA5083-H116 were proposed by Clausen et al. [8]along different directions of the rolled material, and the 0° direction specimen exhibit an opposite fracture strain tendency for various stress triaxialities with others. Eric et al. [9] calibrated the J-C fracture criterion of FV535 steel by averaging Bridgman's analysis and the numerical simulation result. Knowing that only high stress triaxiality is considered in J-C failure criterion, Bao and Wierzbicki [10] studied the fracture ductility in the entire range of stress triaxialities by carrying out a series of upsetting, shear, and tensile on 2024-T351 aluminum alloy, and suggested a segmented failure criterion.However, limited published studies of the fracture criterion coupled with dynamic constitutive mechanical behavior cannot match the increasingly engineering application of AA6082-T6. The objective of this paper is to bridge the gap.

In this paper, quasi-static tensile and compression tests for AA6082-T6 were carried out.A combinedexperimental and simulation method was used to calibrate the J-C fracture model. Further, the tensile tests were simulated to validate the constitutive model and fracture model. Magnifiedfractographs of smooth and notched specimens were recorded by SEM In the end, this paper discussed the mechanical properties of the investigated material under various strain rates and stress triaxialities.

2 Experiment and method

2.1 Experiment procedure and materials

2.1.1 Quasi-static tensile and compression tests

Experiments conducted in this study consist of axial tensile tests, axial compression tests and notchedspecimen tensile tests. The former two groups were set to obtain the strain-stress data of aluminum alloy AA6082-T6, and the last one is for the influence of stress triaxiality. Three repeated experiments in every case were conducted in tension and compression loading test respectively to ensure the test reliability.

The chemical compositions (in wt.%) of aluminum alloy AA6082-T6 used in this study are listed in Table 1.The original material was rolled sheet, and all the specimens for tension experimentwere cut from sheet withthe length direction of the specimens coincident with the rolling direction of the sheet. For quasi-static ($0.0001s^{-1}$) tension tests, the rectangularcross sectiondog-bone specimenswere used with gauge length of 259mm, minimum width of 20mm and thickness of 20mm,as shown in Fig. 1.Cylindrical specimens with gauge length of 20mmand diameter of 6mmwere used for quasi-static compression tests.

(a) (b)

Fig. 1Flat dog-bone specimens (a) geometry (b) specimens (unit: mm).

The tensiletests were performed by MTS electronic universal testing machine (shown in Fig. 2.) at room temperature 20 ℃.The specimens were clamped with a wedge-shaped clamp in tension experiments, as shown in Fig. 2. The displacement was measured by an extensometer with the resolution of 0.5μm in tension test while in compression experiments MTS compression testing machine was used and cylindricalspecimens were placed on highly polish high strength steel plate as shown in Fig. 3.

Table 1 The chemical compositions of aluminum alloy 6082.

Chemical element	Si	Fe	Cu	Mn	Mg	Cr	Zn	Ti
wt.%	0.8	0.5	0.1	0.7	0.9	0.25	0.2	0.1

Fig. 2 MTS electronic universal testing machine.

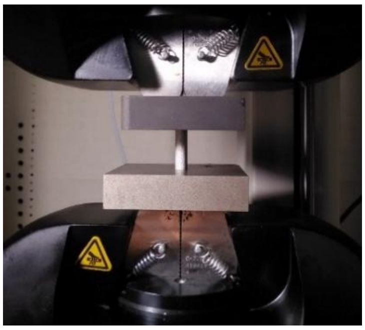

Fig. 3Cylindrical specimens sandwiched in MTS compression testing machine.

The true stress and true strain (respectively denoted as $\sigma_t$and ε_t) are given by the following equations

$$\sigma_t(t) = \sigma_e(t)(1 + \varepsilon_e(t)) \quad (1a)$$

$$\varepsilon_t(t) = ln(1 + \varepsilon_e(t)) \quad (1b)$$

2.1.2 Notched specimen tensile tests

Studies [13-19] have been performed in the past that proved fracture ductility depends markedly on the triaxiality of the stress state.The triaxiality is usually represented by the dimensionless stress triaxiality ratio η, which is defined as

$$\eta = \frac{\sigma_m}{\sigma_{eq}} = \frac{(\sigma_1+\sigma_2+\sigma_3)/3}{\sqrt{\frac{(\sigma_1-\sigma_2)^2+(\sigma_2-\sigma_3)^2+(\sigma_3-\sigma_1)^2}{2}}} \quad (2)$$

where σ_m is the hydrostatic stress, σ_{eq} is the von Mises equivalent stress, and σ_1, σ_2, $\sigma_3$represent three principal stresses. For a uniaxial stress state where σ_1 is the only non-zero component, stress triaxiality $\eta = 1/3$.Hancock and Mackenzie [15] carried out a series oftensile tests on round pre-notched steel specimens. The initial stress triaxiality was calculated according to Bridgman's [14] analysis in their study.

$$\eta = \frac{1}{3} + ln(\frac{r}{2R} + 1) \quad (3)$$

where, r is the radius of the minimum cross-section and R is the radius of the circumferential notch.As Eq. (3) shows, for round pre-notched specimens the value of stress triaxiality increases when the radius of the notch decreases. To investigate the relation between fracture strain and stress triaxiality of AA6082-T6, three types of flat specimens with different notchsize (notch radius 10mm, 40mm, 90mm respectively) were machined (Fig. 4) for tensile test. Because of the different cross-section geometry of round specimen and flat specimen, Bridgman's analysis is not suitable here. But the magnitudeofthe notch radius has the same influence on the stress triaxiality. That is, the specimen with the smaller notch radius has the higher value of the stress triaxiality.

For every type of pre-notched specimen, tensile tests under quasi-static tensileloading were performed. The experiment condition is exactlysame with smooth specimen tensile tests as previously stated.

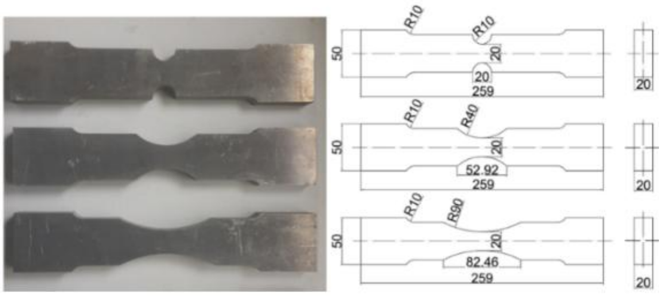

Fig. 4Geometry anddimensions of pre-notched specimens (unit: mm).

2.2 Materialmodel

2.2.1 Johnson-Cook fracture model

Johnson and Cook proposed a fracture model in which the equivalent plastic fracture strain ε_f is dependent on strain rate and temperature in addition to stress triaxiality. The general expression for the equivalent plastic strain at fracture given by J-C failure model is

$$\varepsilon_f = [D_1 + D_2\, exp(D_3\eta)][1 + D_4 ln\dot{\varepsilon}^*][1 + D_5 T^*] \quad (4)$$

The constants D_1, D_2, D_3 are determined from the quasi-static tests on smooth and notched axis symmetric specimens.In present study, all tests were conducted under room temperature, temperature influence on fracture strain is thus neglected. The strain rate effect parameter is neglected as well. The J-C fracture model expression without temperature effect then is simplified as Eq. (5) where only three parameters need to be determined.

$$\varepsilon_f = D_1 + D_2 exp(D_3\eta) \quad (5)$$

2.2.2 Calibration ofJohnson-Cook fracture model

During tensile tests, strain field is not homogeneously distributed throughout the whole specimen and the maximum strain occurs on the fracture surface. Constant volume of the specimen and homogenous strain over the fracture surface are assumed and then the fracture strain [11] could be obtained through

$$\varepsilon_{eq}^f = ln\left(\frac{A_0}{A_f}\right) = ln(\frac{a_0 b_0}{a_f b_f}) \quad (6)$$

Where A represent minimum sectional area on the specimen. a and b are the width and the height ofspecimens at minimum sectional area respectively.The subscript “0” and “f” represent before and after the test.

Previous works [12-15] have calculated stress triaxiality of round specimens withBridgman’s formulation (Eq. (3)) which is a valid method to obtainthe stress triaxiality over the minimum cross section accurately. Actually, stress triaxiality of the specimen is not a constant value in the plastic strain process [8, 9]. The stress triaxialitychanges with the geometry evolution of a specimens What’s more, the stress triaxiality distributes nonuniform in the minimum sectional area. Thus, stress triaxiality is a complicated function of equivalent strain and space distribution.In the fracture model parameter fitting process, computing method of the values of specimen stress triaxiality ηcorresponding to the fracture strain plays a decisive role to the fitting result. However, Bridgman's formulation is not suitable for flat specimens either. For these reasons, a different technique is required to obtain a reasonable value of stress triaxiality. Bao and Wierzbicki [9] used a new concept of average stress triaxiality η_{av}. The average stress triaxiality is interpreted by the integration of stress triaxiality with respect to equivalent plastic strain as shown in Eq. (7).

$$\eta_{av} = \frac{1}{\varepsilon_f} \int_0^{\varepsilon_f} \eta d\varepsilon_{p,eq} = \frac{1}{\varepsilon_f} \sum_{t=0}^{t=t_f} \eta_t (\Delta\varepsilon_{p,eq})_t \qquad (7)$$

where t_f is time to fracture; $\varepsilon_{p,eq}$ is the equivalent plastic strain. The average stress triaxiality is the summation of stress triaxiality multiplied by the incremental equivalent plastic strain at t_f.

In this work, a method combining experimental data and numerical simulationswas applied to obtain the stress triaxiality history of the entire experiment process. The procedures is as follow:

Step1: Compute numerical simulations of the tested specimens with a suitable non-linear finite element code. Confirm that the engineering stress-strain curves obtained from FE simulation and tests are coincident each other. It should be noted that fracture criterion is not used.

Step 2: Identify the engineering failure strain by comparing numerical and experimental curves a. Find the time step of specimen fracture.

Step 3: Obtain stress triaxiality and equivalent plastic strain histories in the most critical elements, which is defined as those for which the values of stress triaxiality and equivalent plastic strain are most unfavorable. One should be noted that there is an assumption for the original J-C calibration[7], stress triaxiality and equivalent plastic strain distribute homogeneously over the minimum cross section area.

Step 4: Obtain the equivalent fracture plastic strains of the most critical elements.

Step 5:Once the history of stress triaxiality obtained, the initial stress triaxiality can be read. Calculate the average stress triaxiality with Eq. (7). Then, two sets of stress triaxiality, i.e. the initial and average respectively, are obtained.

Step 6: Plot the stress triaxiality versus the equivalent fracture plastic strains. Formulate the relation between the stress triaxiality and the equivalent fracture plastic strains.

By using the above methodology, two sets of points in stress triaxialityversus equivalent fracture plastic strains space can be obtained. One of the sets is the lower fracture limit.And another is the proposed calibration point sets. In fact, according to previous works[8-10], with the necking developing the stress triaxiality in minimum section area is increasing. And high stress triaxiality contributes to advanced fracture. Therefore, the initial stress triaxiality are supposed to corresponds to the lower fracture limit while another set points corresponding to the average stress triaxiality, which is closer to the actual situation. One should be stressed here is that in stress triaxiality versus equivalent fracture plastic strains space, the initial stress triaxiality corresponds to the equivalent fracture plastic strains calculated with Eq. (6) which is considered to be the average value of equivalent fracture plastic strains over the minimum cross section. On the one hand, the set of points has been designated as lower fracture limit. On the other hand, the set of points obtained in common way can also contrast with the proposed calibration. The reason of choosingthe most unfavorable elements for obtaining the stress triaxiality and equivalent plastic strain histories, instead of the average stress triaxiality,is that fracture takes place once some element has failed.

3 Results

3.1 Stress-strain curves under tensile and compression loading

The engineering stress-strain curves of AA6082-T6 under quasi tension and compression are shown in Fig. 5. In the beginning of tensile loading, the material shows linear elastic behavior within the elastic regime. When the stress reached yield limit (about 270Mpa) which means the material come into the plastic stage the increase tend to be much gentle till the stress meet ultimate strength. The ultimate strength for AA6082-T6 is 351.51 MPa. Compared with tensile loading procedure, the material under compression loading has a lasting elastic stage, a relatively greater yield stress and a greater ultimate strength, 295.78 MPaand 381.90 MPa respectively.

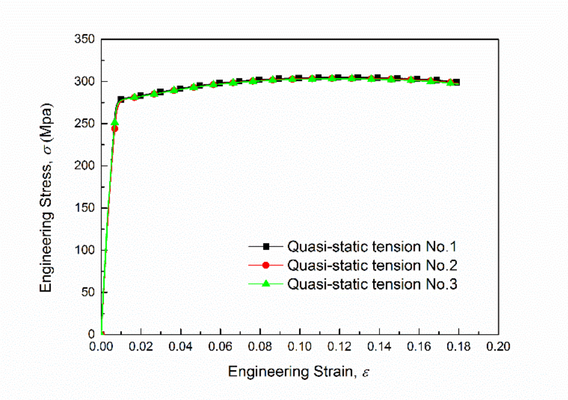

(a)

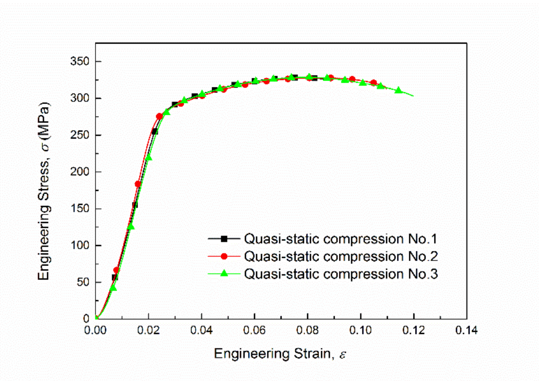

(b)

Fig 5 Engineering stress-strain curve under quasi-static (a) tension and (b) compression test

3.2 Numerical simulations of smooth and notched specimens

In this paper, a non-linear finite element code, ABAQUS/Standard wasused for the numerical simulations. Four smooth and notched specimen models were simulated. The experimental data obtained in Section. 3.1wasinput. It is worthyofnote that no failure criterion is introduced due to the calibration aim of simulation instead of validation.

Only the 1/4 of specimens is modeled to reduce the computing time. The element type is the three dimensional hexahedral element with reduced integration (C3D8R). The meshes of the finite element models are shown inFig. 6.Mesh refinement technique is adopted near the fracture zone. Fig. 7 shows a typical finite element meshes of notched specimen model with notch radius of 10mm. The mesh of the smooth specimen has 119120 elements while the specimens with notch radius,R=90mm,R=40mm and R=10mm, have 75400, 34000 and 54440 elements respectively.

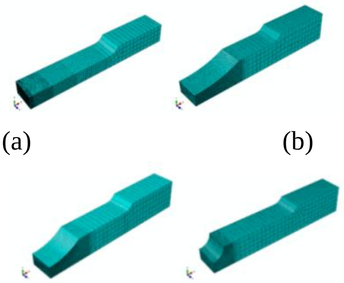

(a) (b) (c) (d)

Fig.6. Finite element model meshes of (a) smooth and notched specimens with notch radius of (b) 90mm, (c) 40mm and (d) 10mm for ABAQUS/Standard.

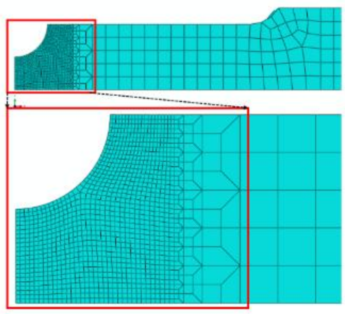

Fig.7. Typical finite element meshes of notched specimen model with notch radius of 10mm.

The engineering stress-strain curves from numerical simulations agree well with those from experiments as shown in Fig. 8. By simulating the processes of tensile tests, spatial distribution of the stress triaxiality and equivalent plastic strain from the beginning to the fracture can be obtained. Fig.9 shows stress triaxiality and equivalent plastic strain profile of smooth and notched specimens along two perpendicular axes over the minimum cross section. The profile is obtain from ABAQUS/Standard numerical simulations at the step time of fracture. The stress triaxiality values over the minimum cross section decrease from the center of the rectangle cross section to the edge. However, the stress triaxialities of the edges for different specimens are in a rough range from 0.33 to 0.4 where the gradient is not as marked as the center. Seeing from the space, plastic deformation concentrates nearby the minimum section area, and the maximum value of stress triaxiality is located in the center of the minimum section area almost throughout the whole plasticstrainstage, as expected. And the stress triaxiality values along two perpendicular axis show a small difference. The equivalent plastic strain shows the same tendency as the stress triaxiality. Nonetheless, as shown in Fig.9 (b), the variation of equivalent plastic strain along the transverse axis of 10mm notch radius specimen exhibit an opposite behavior, which is opposite with the variation along the transverse axis too and may lead to an advanced failure. After all, due to the marked difference of the stress triaxiality level between the cross section center and the notch surface along the transverseaxis for the 10mm notch radius specimen, failure is supposed to begin with the center of the minimum cross section. In conclusion, the elements that failure begin with located in the center of the minimum cross sections of specimens.

The two sets of points in the equivalent plastic strain verse the stress triaxiality space are plotted in Fig.10.The first set of points given by acommon method, in which the initial stress triaxiality and the fracture strain calculated with Eq. (6)were adopted. All the fracture area ratios (A_0/A_f) of minimum sectional area and the calculated fracture strain ε_{eq}^{f} are listed in Table 2 as well as the fracture strains from numerical simulations,and the data are all averaged results of repeated tests. With the same height and width at the minimum cross section, a_0 and b_0 are both 20mm for each specimen. And the second set is the averaged stress triaxiality versus the fracture strain obtained from ABAQUS/Standard numerical simulation. Comparing with the latter set points the points obtained from common way incline to locate below, which implies a more conservative fracture criterion. Stress triaxiality histories of the critical elements are plotted as well. These curves exhibit a generally increasing tendency with the development of plastic strain for every type of specimens. This effect is more marked for specimens with larger initial stress triaxialities

3.3 Johnson-Cook fracture model constant identification

The construction of the J-C fracture model implies that five constants must be identified (see Eq. (4)). In present work, the effect of temperature is not taken into consideration. Thus, the constant in the temperature-dependent factor is neglected, then the formula, with four constants left to identify, issimplified as Eq. (6). The calibration of the J-C fracture model is built using the average stress triaxiality versus equivalent fracture plastic strain dataset while another J-C fracture model (the lower limit) is built using the initial average stress triaxiality versus equivalent fracture plastic strain data set..

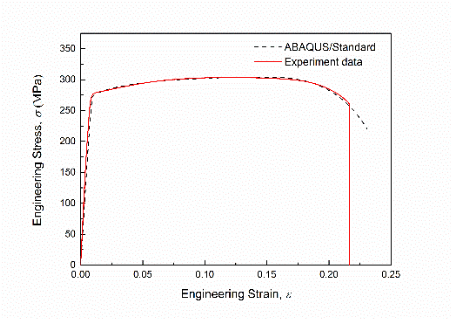

(a)

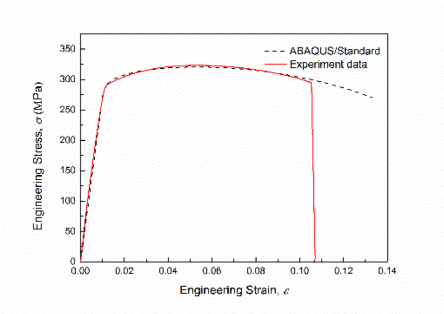

(b)

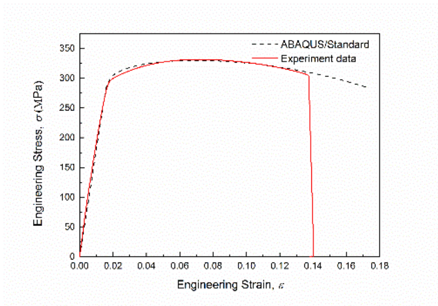

(c)

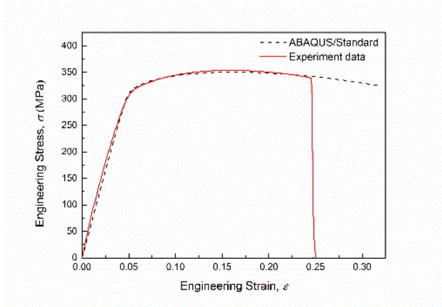

(d)

Fig. 8. Engineering stress- strain curves from experiments and ABAQUS/Standard numerical simulations for (a) smooth specimen, (b) 90mm, (c) 40mm and (d) 10mm notch radius specimens.

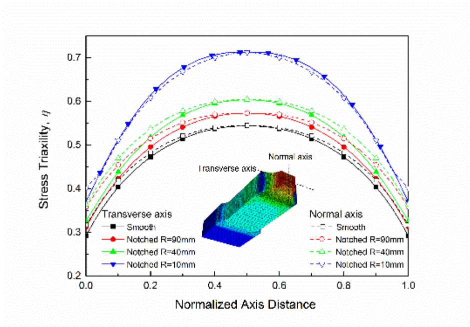

(a)

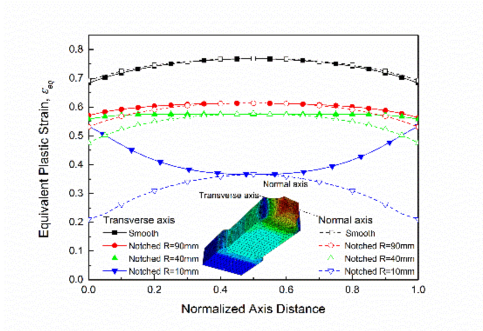

(b)

Fig. 9.(a) Stress triaxialities and (b) equivalent plastic strain profile of smooth and notched specimens over the minimum cross section at the fracture time step.

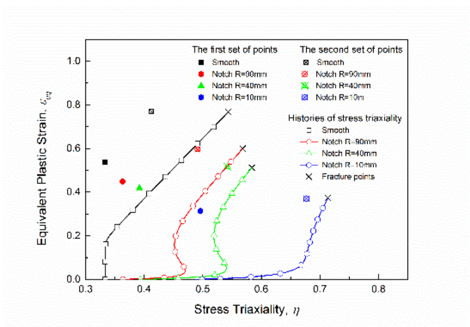

Fig. 10.The two sets of points and histories of the stress triaxiality in quasi-static tensile tests.

Similar parameter fitting processes have been done by minimizing the residuals with success [12, 13]. In present work, the same method is adopted. The quasi-static tensile test data of smooth and notched specimens is used to fitting the first three constants. The constants obtained with the two data sets are shown Table 3.

Table 2 Fracture reduction ratio (A0/Af) and comparison of equivalent plastic strains to fracture between calculated results from Eq. (6) and numerical simulations.

Specimen types	Test strain rate (s^{-1})	A_f (mm^2)	A_0/A_f	ε_{eq}^f	ε_{eq}^{f-s}
Smooth	Quasi-static	217.984	1.835	0.607	0.768
	0.001	234.055	1.709	0.536	0.612
	0.01	232.558	1.702	0.532	0.585
	0.1	243.457	1.643	0.499	0.553
	1	244.051	1.639	0.494	0.545
Notched R=90mm	Quasi-static	255.265	1.567	0.449	0.59977
Notched R=40mm	Quasi-static	263.158	1.520	0.419	0.51229
Notched R=10mm	Quasi-static	292.398	1.368	0.313	0.37395

ε_{eq}^{f-s}: The equivalent plastic strain obtained from numerical simulations.

Table 3 J-C fracture model parameters for the common method and calibration

Parameter	D_1	D_2	D_3
Common method	0.26862	9.20158	-10.6552
Calibration	0.21125	3.91116	-4.72526

4 Discussion

4.1 Validation of the J-C fracture model

In this paper, a calibration methodology is proposed to obtain a simplified J-C fracture model to describe the ductility fracture more accurately. Previous works have built J-C fracture models for various materials with success. A common method is used to obtain the data set of stress triaxialities and equivalent fracture plastic strain that take the initial stress triaxiality (given by Bridgman's analysis Eq. (4)) and equivalent fracture plastic strain calculated with Eq. (6). However, this method may lead to a relatively conservative result due to the underestimate of global stress triaxialities. For this reason, some calibrations for the J-C fracture model were proposed. Bao et al. [10] proposed to integrate the stress triaxiality of entire process with respect to equivalent plastic strain as shown in Eq. (7). Such method is used by Choung et al. [16, 17] to estimate the failure strain of EH36, and a good prediction was provided. Eric et al. [9] suggested an approach byaveraging two data sets, the "lower" and the "upper" fracture limits. They took the data set from common method as the "lower" limit, and obtain the "upper" data set from numerical simulations where the stress triaxialities and the equivalent plastic fracture strains of the critical elements at fracture time step were used. Such calibration only through averaging the two limits seems closer to reality than the common method, however, the accuracy may not enough. Here, the two methods were combined to calibrate the J-C fracture model. The average stress triaxiality is used and the equivalent plastic fracture strains are obtained from numerical simulations at the fracture time step.Fig. 11 shows the two model in the stress triaxiality versus equivalent plastic strain space. What is noteworthy is that the relation is given only in the region of high stress triaxiality due to the limitation of J-C fracture model [10]. The calibrated J-C fracture model was added in the numerical simulations of the quasi-static tensile tests for smooth and notched specimens. Also, the J-C fracture model was used in ABAQUS/Explicit simulations for comparison. Fig. 12 shows the fracture process of the smooth specimen in the numerical simulation.The fracture simulation gives a depiction of the stress triaxiality distribution and fracture process. When the equivalent plastic strain reach the fracture strain elements are deleted automatically. It can be seen that failure started in the center area of the minimum cross section due to the high level of the stress triaxiality and spread towards the edge, and the four corners were sheared to fracture at last.

The engineeringstress-strain curves of smooth and notched specimens under quasi-static strain rate, obtained from experiments and numerical simulations respectively, are plotted in Fig. 13 to validate the calibration of J-C fracture model.The common J-C fracture model shows relatively “conservative” estimating on the ductility of AA6082-T6 alloy as expected. The underestimation reaches to an averaging extent of 13.50%. And the average error of the engineering fracture strain after calibration is 6.05% which is a great improvement on fracture strain estimation. The results give an evidence that the calibration methodology can improve the accuracy of J-C fracture model effectively.

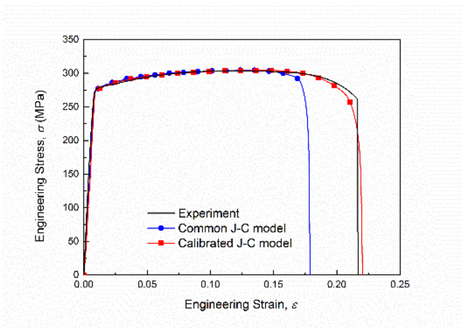

(a)

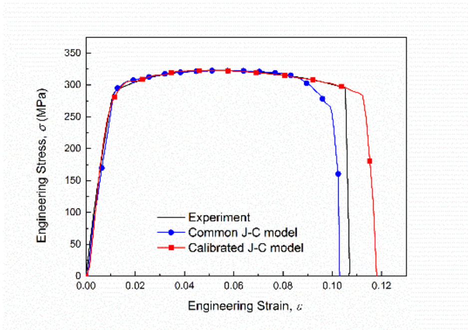

(b)

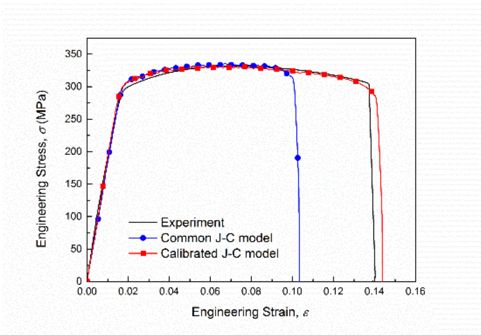

(c)

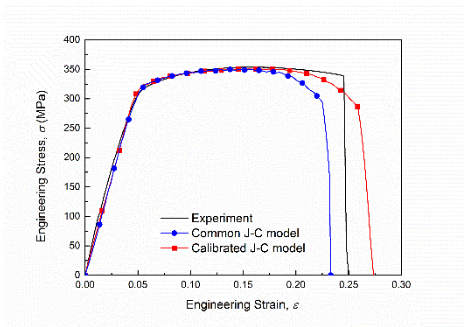

(d)

Fig. 13. Engineering stress-strain curves from experiments and ABAQUS/Explicit numerical simulations for (a) smooth specimen, (b) 90mm, (c) 40mm and (d) 10mm notch radius specimens.

4.2 Fractography analysis

From the results of a series of tensile tests, it is found that AA6082-T6 exhibits an excellent ductility, with an elongation of 10% to 25%. A number of studies have been done on ductility damage and ductility fracture [18-21]. It is a common view that the dimple fracture(experiencing the process of the nucleation, growth, and coalescence of voids) and shear fracture (developed from shear band localization) are two primary fracture forms for the ductile material. Fig. 14 shows the smooth and notched specimens after fracture at quasi-static strain rate. Typical cup-and-cone form fracture surfaces are shown. The central zone of the fracture surface is ductile normal fracture full of bumps and hollows while the rest area is shear fracture with surface along the maximum shear stress plane, namely an angle of 45degree to the tensile axis.The SEM fractographs of the two areas in the smooth specimen fracture surface are shown in Fig. 14.Fig. 15 (a) exhibits a typical nucleation-growth-coalescence process of ductility fracture, where a lot of voids and dimples can be observed. In the central zone, the stress triaxiality is supposed to be higher than the area close to the specimen surface. When a ductile material is subjected to hydro static stress,micro-voids nucleated in the central zone giving priority to impurities and second-phase particles,then grow bigger with the development of deformation, at last grown voidcoalescence leads to many micro cracks. When the micro cracks link up and expand to the area close to the specimen surface shear fracture take place. Fig. 15 (b) shows shear fracture mode in the fracture surface.

Fig. 14Notched specimens (notch radius 10mm, 40mm, and 90mm from left to right) and smooth specimen after fracture at quasi-static strain rate.`

SEM micrographs of smooth and notched specimens fracture surface under quasi-static are compared in Fig. 16. The smooth specimen show relatively little and small dimples. As the radius of notches decrease, i.e., the stress triaxiality increases, bigger dimples are shown. The reason is that in the nucleation stage, voids grow rapidly due to high stress triaxiality. High hydrostatic pressure likely result in large dimples which may accelerate the dimple fracture. And low hydrostatic pressure leads to shear band localization and further cause shear fracture.

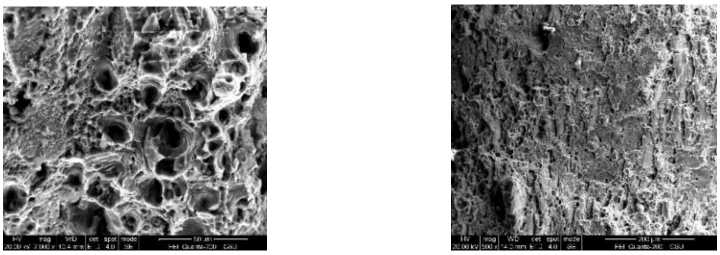

(a) (b)

Fig. 15. (a) Dimple fracture and (b) shear fracture in smooth specimen fracture surface

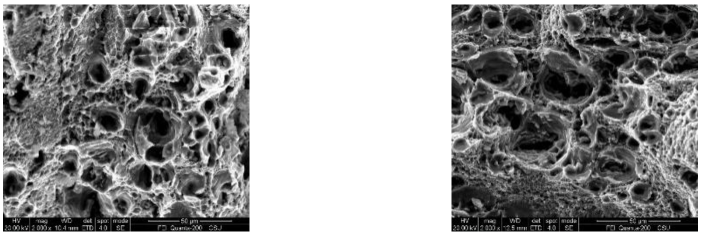

(a) (b)

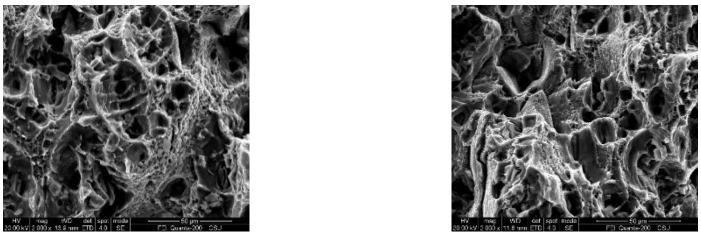

(c) (d)

Fig. 16.Fracture surfaces of four kind of specimens (a) smooth, (b) notched R=90mm, (c) notched R=40mm, and (d) notched R=10mm.

Conclusions

In this paper,a series of tests were carried out to investigate the fracture behavior of AA6082-T6 under various different stress state. Numerical simulations based on FEA were successfully performed. Primary conclusions can be drawn as follows:

- A calibration methodology of J-C fracture model was proposed by using the average stress triaxiality and the equivalent plastic fracture strain of the critical elements (in the central zone of the minimum cross section).
- Numerical simulations based on FEA were performed in ABAQUS. By simulating the tensile process, it was proven that the stress triaxiality over the fracture cross section in the central zone is the highest, where the failure begins first. The calibrated J-C fracture model was proven to be valid in predicting the fracture strain of AA6082-T6 alloy.
- Ductility fracture is the main fracture form in tensile test for the present material. Dimple fracture appears in the central of the minimum cross section due to the high level of stress triaxiality and the rest area was sheared to fracture. As initial triaxiality increased, the dimple size over the fracture surfaces become larger. It may be caused by the rapid growth of voids in the nucleated stage due to high stresstriaxiality.

Acknowledgements

This work was supported by the National Natural Science Foundation of China (No. 51405517 and U1334208) and the Natural Science Foundation of Hunan (2015JJ3155).

References

[1] Spigarelli S, Evangelista E, McQueen HJ. *Study of hot workability of a heat treated AA6082 aluminum alloy*. Scr Mater 2003;49:179–83.

[2] Tranə E, Rotariu AN, Lixandru P, Matache LC, Enache C, Zecheru T. *Experimental and numerical investigation on 6082 0 temper aluminium alloy cartridge tubes drawing.* J Mater Process Technol 2015;216:59–70.

[3] Chen Y, Clausen AH, Hopperstad OS, Langseth M. *Stress-strain behaviour of aluminium alloys at a wide range of strain rates.* Int J Solids Struct 2009;46:3825–35.

[4] Ludwik P, Scheu R.*Ueber Kerbwirkungen bei Flusseisen.*Stahl u. Eisen 1923;43:999–1001.

[5] Bridgman PW.*Studies in Large Plastic Flow and Fracture*. New York: McGraw-Hill; 1952.

[6] Hancock JW, Mackenzie AC.*On the mechanisms of ductile failure in high-strength steels subjected to multi-axial stress-states. J. Mech. Phys.* Solids 1976;24:147–160.

[7] Johnson GR, Cook W a. *Fracture characteristic of three metals subjected to various strains, strain rates, temperatures and pressures*. Eng Fract Mech 1985;21:31–48.

[8] Clausen AH, Børvik T, Hopperstad OS, Benallal A. *Flow and fracture characteristics of aluminium alloy AA5083-H116 as function of strain rate, temperature and triaxiality.* Mater Sci Eng A 2004;364:260–72.

[9] Erice B, Gálvez F, Cendón DA, Sánchez-Gálvez V. *Flow and fracture behaviour of FV535 steel at different triaxialities, strain rates and temperatures*. Eng Fract Mech 2012;79:1–17.

[10] Bao Y, Wierzbicki T. *On fracture locus in the equivalent strain and stress triaxiality space*. Int J Mech Sci 2004;46:81–98.

[11] Wierzbicki T, Bao Y, Lee YW, Bai Y. *Calibration and evaluation of seven fracture models*. Int J Mech Sci 2005;47:719–43.

[12] Hu DY, Meng KP, Jiang HL, Xu J, Liu RR. *Strain rate dependent constitutive behavior investigation of AerMet 100 steel*. Mater Des 2015;87:759–72.

[13] Trajkovski J, Kunc R, Pepel V, Prebil I. *Flow and fracture behavior of high-strength armor steel PROTAC 500*. Mater Des 2015;66:37–45.

[14] Børvik T, Hopperstad OS, Dey S, Pizzinato E V., Langseth M, Albertini C. *Strength and ductility of Weldox 460 E steel at high strain rates, elevated temperatures and various stress triaxialities.* Eng Fract Mech 2005;72:1071–87.

[15] Li HY, Li YH, Wang XF, Liu JJ, Wu Y. *A comparative study on modified Johnson Cook, modified Zerilli-Armstrong and Arrhenius-type constitutive models to predict the hot deformation behavior in 28CrMnMoV steel.* Mater Des 2013;49:493–501.

[16] Choung J, Shim CS, Song HC. *Estimation of failure strain of EH36 high strength marine structural steel using average stress triaxiality*. Mar Struct 2012;29:1–21.

[17] Choung J, Nam W, Lee D, Song CY. *Failure strain formulation via average stress triaxiality of an EH36 high strength steel.* Ocean Eng 2014;91:218–26.

[18] Le Roy G,Embury JD,Edwards G,Ashby MF. *A model of ductile fracture based on the nucleation and growth of voids*.Acta Metallurgica 1981;8:1509-1522.

[19] Pardoen T, Hutchinson JW. *Extended model for void growth and coalescence*. J Mech Phys Solids 2000;48:2467–512.

[20] Majzoobi GH, Mahmoudi AH, Moradi S. *Ductile to brittle failure transition of HSLA-100 Steel at high strain rates and subzero temperatures*. Eng Fract Mech 2016;158:179–93.

[21] Malcher L, Andrade Pires FM, César de Sá JMA. *An assessment of isotropic constitutive models for ductile fracture under high and low stress triaxiality.* Int J Plast 2012;30-31:81–11